Journal of Magnetic Resonance **144,** 96–107 (2000)
doi:10.1006/jmre.2000.2033, available online at http://www.idealibrary.com on IDEAL®

Correlation Time and Diffusion Coefficient Imaging: Application to a Granular Flow System

Arvind Caprihan and Joseph D. Seymour

New Mexico Resonance, Albuquerque, New Mexico 87108

Received September 8, 1999; revised January 21, 2000

A parametric method for spatially resolved measurements for velocity autocorrelation functions, $R_u(\tau) = \langle u(t)u(t+\tau)\rangle$, expressed as a sum of exponentials, is presented. The method is applied to a granular flow system of 2-mm oil-filled spheres rotated in a half-filled horizontal cylinder, which is an Ornstein–Uhlenbeck process with velocity autocorrelation function $R_u(\tau) = \langle u^2\rangle e^{-|\tau|/\tau_c}$, where τ_c is the correlation time and $D = \langle u^2\rangle\tau_c$ is the diffusion coefficient. The pulsed-field-gradient NMR method consists of applying three different gradient pulse sequences of varying motion sensitivity to distinguish the range of correlation times present for particle motion. Time-dependent apparent diffusion coefficients are measured for these three sequences and τ_c and D are then calculated from the apparent diffusion coefficient images. For the cylinder rotation rate of 2.3 rad/s, the axial diffusion coefficient at the top center of the free surface was 5.5×10^{-6} m^2/s, the correlation time was 3 ms, and the velocity fluctuation or granular temperature $\langle u^2\rangle$ was 1.8×10^{-3} m^2/s^2. This method is also applicable to study transport in systems involving turbulence and porous media flows.

Key Words: **velocity autocorrelation; correlation time; diffusion coefficient; pulsed-field-gradient; granular flows.**

INTRODUCTION

A magnetic resonance imaging (MRI) method has been developed to spatially measure the parameters of any velocity autocorrelation function that can be expressed as a sum of exponentials. The nuclear magnetic resonance (NMR) method used is a modification of the original pulsed gradient methods by Stejskal and Tanner (*1*) to probe diffusion processes. These methods and their applications have been discussed by Callaghan (*2*) and in more recent reviews (*3, 4*). Ours is a general NMR method that can be applied to problems such as turbulence and porous media flows. In this paper we apply it to a granular flow system consisting of 2-mm spherical particles rotated in a half-filled horizontal cylinder. We have previously made MRI measurements of the velocity field (*5*), axial segregation (*6*), apparent diffusion coefficient images (*7*), and time-dependent diffusion coefficient images (*8*) in granular flow systems. In this paper we present a method to calculate the correlation time and the diffusion coefficient corresponding to the random motion of granular particles from apparent diffusion coefficient images.

Granular flows are of significant technological and scientific interest. This is due to their ubiquitous presence in geophysical systems and major industries, such as foods, pharmaceuticals, and power, and because of their complex behavior which encompasses solid-, liquid-, and gas-like states and includes pattern formation and self-organized criticality (*9*). A characteristic feature of granular flow is the discrete nature of the particles and the presence of dissipative inelastic collisions. Continuum mechanics methods modified with concepts from the kinetic theory of gases have been developed (*10–12*) to model granular flow. The concept of granular temperature, associated with the variance of the fluctuating component of the velocity, is introduced to model flow and is incorporated into the system energy balance equation (*12*). Savage and Dai (*13*) have used molecular dynamics simulations and shown that particle collisions can be modeled by a near exponential velocity autocorrelation function in shear flow. In segregation/mixing studies of inhomogeneous particles, either in the rotating cylinder or in a vibrated layer, an important phenomena is that of a mixture of particles with different diffusivities causing particle segregation and pattern formation. A diffusion coefficient describing this particle migration has been used to develop segregation theories (*14–16*). Thus, a noninvasive nuclear magnetic resonance (NMR) technique to spatially image the stochastic properties of particle motion will be of great value. MRI can make spatially resolved 3D velocity fluctuation measurements deep within the bulk of opaque materials, unlike a recently proposed technique of diffusing-wave spectroscopy (*17*), which makes use of multiple scattered light.

We model the particle velocity by a stationary stochastic process with mean velocity V and a random fluctuating velocity u, such that that the velocity autocorrelation function is $R_u(\tau) = \langle u(t+\tau)u(t)\rangle$. The formal force balance for the system can also be expressed in terms of a generalized Langevin equation (*18*),

$$m\frac{d}{dt}u(t) = -m\int_{-\infty}^{t} h(t-s)u(s)ds + f_r(t), \qquad [1]$$

1090-7807/00 $35.00

where m is the mass of the particle, $h(t)$ is the memory function which incorporates friction effects, and $f_r(t)$ is the random force. The autocorrelation function $R_u(\tau)$ of $u(t)$ can be related to the memory function $h(t)$ and the forcing function properties through the fluctuation dissipation theorem (*18*). The method we discuss in this paper consists of assuming a parametric form for $R_u(\tau)$ and estimating its parameters. The same technique can also be applied to measure the parameters of the memory function.

Another important tool for studying dynamics, mixing, and transport in systems with random or nonlinear advection is the time-dependent diffusion coefficient

$$D(\Delta) = \frac{\langle (x(\Delta) - x(0))^2 \rangle}{2\Delta}, \qquad [2]$$

where $x(\Delta)$ is the position of the particle at time Δ and $\langle (x(\Delta)\rangle - x(0))^2 \rangle$ is the mean squared displacement or position variance (*19*). Because the particle displacement can be calculated from the velocity, the time-dependent diffusion and velocity autocorrelation are related for a stochastic process by

$$D(\Delta) = \int_0^\Delta \left(1 - \frac{\tau}{\Delta}\right) R_u(\tau) d\tau. \qquad [3]$$

The diffusion coefficient is defined to be the long time limit of $D(\Delta)$,

$$D = \lim_{\Delta \to \infty} D(\Delta) = \int_0^\infty R_u(\tau) d\tau. \qquad [4]$$

NMR is a powerful technique for probing particle dynamics because the diffusion coefficient measured by NMR with narrow (impulse like) bipolar pulsed gradients (*2, 4*) and time separation Δ is the time-dependent diffusion coefficient $D(\Delta)$. If the gradients are not impulses, then NMR measures an apparent time-dependent diffusivity whose analytical expression can be calculated provided we know the analytical model for $R_u(\tau)$ (*20*).

The average correlation time for a process with velocity autocorrelation function $R_u(\tau)$ is defined by (*18*)

$$\tau_c = \int_0^\infty R_u(\tau) d\tau / R_u(0), \qquad [5]$$

and the velocity fluctuation intensity, referred to as the granular temperature in granular flow studies, by $\langle u^2 \rangle = R_u(0)$ (*13*). It then follows that

$$D = \langle u^2 \rangle \tau_c. \qquad [6]$$

We develop a method for estimating parameters of the velocity autocorrelation function $R_u(\tau) = \langle u^2 \rangle e^{-|\tau|/\tau_c}$ of the Ornstein–Uhlenbeck (O–U) process (*18*), which describes the velocity of a Brownian particle. Three pulse sequences will be used: (a) a standard bipolar pulsed gradient spin-echo sequence (PGSE), (b) its repeated version with two cycles, and (c) a flow compensated pulsed gradient spin-echo sequence (*21*), also referred to as double PGSE elsewhere (*2, 4*). We use the nomenclature of "flow compensated pulse gradient spin-echo sequence" rather than double PGSE to avoid confusion with the repeated PGSE sequence. The flow compensated pulsed gradient sequence has its first moment zero, $\int tg(t)dt = 0$, where $g(t)$ is the effective gradient and is akin to the even spin echo. It has the property that the magnetization of a spin moving with constant velocity accumulates no net phase during the sequence, an effect first observed by Carr and Purcell (*22*). deGennes showed that even for stochastic motion with correlations, such as turbulent flow, even echoes refocus spins partially and reduce signal loss (*23*). We use this sensitivity toward correlated motion to improve correlation time measurements. The compensated pulse sequence is also the smallest subset of the time-modulated gradient pulse sequences considered by Callaghan and Stepisnik (*24*). They developed their theory in the frequency domain, while we present a technique for estimating the parameters of $R_u(\tau)$ in the time domain in this paper.

Stepisnik (*20*) has derived equations for the apparent diffusion coefficient and applied them to experimental data on polymer diffusion. He considered both the O–U process and an exponential memory function. We derive similar expressions for the compensated and the repeated pulsed gradient sequence. In turbulence studies Gao and Gore (*25*) have applied an exponential velocity auotcorrelation function. Kuethe and Gao (*26*) considered a parametric form $D(\Delta) = D_t(1 - e^{-\Delta/\tau_c})$, and compared their model to Gao and Gore's (*25*), at first and second echoes, for their applicability to measure the eddy diffusivity. In this paper our emphasis is on strategies to measure the velocity autocorrelation function of any general form, using the exponential correlation as a template.

Studies of transport phenomena in heterogeneous media apply averaged theories of transport phenomena which model the conveyance of mass, energy, momentum, and electricity within the system. Examples of averaged transport models are found in the kinetic theory of gases, turbulent flow theory, transport theories for porous media, colloidal systems, and multiphase (solid–liquid–gas) suspensions. Mixing occurs in these systems because of nonlinear flow effects and coupling between flow and diffusion. Transport is due to macro scale

velocity fluctuations and is often modeled by dispersion (*27*) or an effective diffusion coefficient (*19*). The dispersion theory is similar to those for diffusion and the same MRI techniques used for measuring the microscopic molecular diffusion coefficient can also be employed for measuring macroscopic dispersion (*28*). The dispersion coefficient has been measured for porous media flows (*29–32*) and Taylor dispersion (*33*). A concept of nonlocal dispersion coefficient has been developed to model transport processes where velocity has fluctuations over a continuum of scales, as in turbulence and fractal porous media (*27*), and NMR methods for its measurement have also been developed (*34*).

THEORY

The principle of this method will be illustrated in terms of the effective gradients $g(t)$ of duration T and zero area ($\int g(t) = 0$). This condition is necessary for the phase of the stationary spins to be refocussed. The phase of the NMR spin is given by

$$\phi(T) = \gamma \int_0^T g(s)x(s)ds = -\gamma \int_0^T \theta(s)u(s)ds, \quad [7]$$

where $\theta(t) = \int_0^t g(s)ds$ and $\theta(T) = 0$ because $\int_0^T g(t)dt = 0$. Following Mitra and Halperin (*35*) we can express $\phi(T)$ in terms of $q = (\gamma g \delta)/(2\pi)$ and the mean position of the particles

$$x_{\delta,t_k} = \frac{1}{\delta} \int_{t_k}^{t_k+\delta} x(s)ds$$

during each gradient pulse of duration δ. For the bipolar gradient pulse pair sequence of Fig. 1A, we have

$$\begin{aligned}\phi(T) &= 2\pi q(x_{\delta,0} - x_{\delta,t_1} - x_{\delta,t_2} + x_{\delta,t_3} + x_{\delta,t_4} - x_{\delta,t_5}) \\ &= 2\pi qX, \end{aligned} \quad [8]$$

where $X = x_{\delta,0} - x_{\delta,t_1} - x_{\delta,t_2} + x_{\delta,t_3} + x_{\delta,t_4} - x_{\delta,t_5}$. $x_{\delta,t_k} = x(t_k)$ is the position of the particle at time t_k for a short δ. X measures the particle displacement in the time Δ between the bipolar gradients for one bipolar pulse. For multiple bipolar pulses of arbitrary polarity, X is a combined measure of particle displacement during each bipolar gradient pulse. Its variance depends on correlations among successive displacements (*4*). In this analysis we repeat bipolar gradient pulses of zero area with arbitrary polarity. A different probing sequence where one gradient pulse is followed by n refocussing gradient pulses has been considered in (*36*) to measure position correlations. Another variation is the 2D velocity exchange experiment (VEXSY), where the amplitude of two pairs of bipolar gradients is stepped independently (*37*).

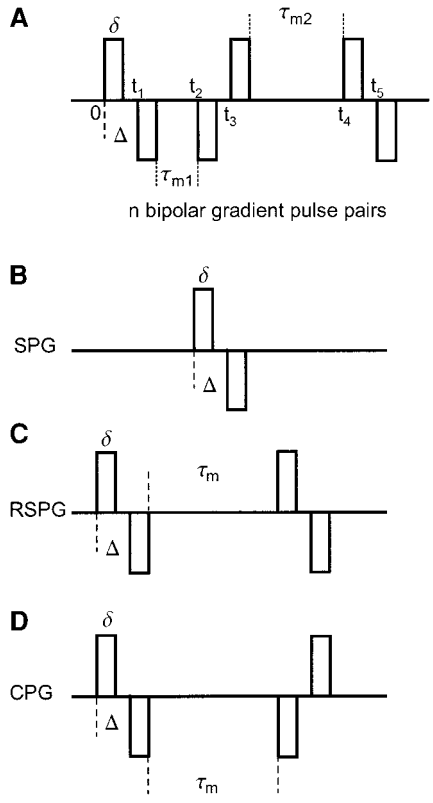

FIG. 1. Effective pulsed magnetic field gradient sequences. (A) A general sequence with n bipolar gradient pulses of arbitrary order. Gradient pulse sequences with different motion probing properties can be designed by controlling the polarity of the bipolar pulses and the mixing times τ_{mk}. (B) The effective gradient for the single pulsed gradient (SPG) experiment. (C) The repeated pulsed gradient (RSPG) sequence. (D) The compensated pulsed gradient (CPG) sequence. Each of the gradient sequences has a different sensitivity to motion dependent on the time scales of the motion and the gradient sequence polarity.

The NMR signal is proportional to $\langle e^{i\phi(T)} \rangle = e^{i\langle\phi\rangle}\langle e^{i(\phi(T)-\langle\phi\rangle)}\rangle$, with its magnitude being given by

$$E = \left|\langle e^{i(\phi(T)-\langle\phi\rangle)}\rangle\right| . \quad [9]$$

Equation [9] can be expanded by cumulant expansion to

$$E = e^{-\langle[\phi(T)-\langle\phi\rangle]^2\rangle_c/2! + \langle[\phi(T)-\langle\phi\rangle]^4\rangle_c/4! - \cdots}, \quad [10]$$

where $\langle x \rangle_c$ stands for the cumulant of x. Expanding cumulants, we get (*18*)

$$E = e^{-\langle[\phi(T)-\langle\phi\rangle]^2\rangle/2! + \{\langle[\phi(T)-\langle\phi\rangle]^4\rangle - 3\langle[\phi(T)-\langle\phi\rangle]^2\rangle^2\}/4! - \cdots}. \quad [11]$$

Equation [11] can also be expressed in terms of q and X as

$$E = e^{-2\pi^2 q^2 \sigma_x^2 + (2\pi^4 q^4((X-\langle X\rangle)^4 - 3(\sigma_X^2)^2))/3 - \cdots}. \quad [12]$$

If $\phi(T)$ has Gaussian distribution, terms higher than second order are zero and we get

$$E = e^{-\sigma_\phi^2/2}, \quad [13]$$

where $\sigma_\phi^2 = \langle(\phi(T) - \langle\phi\rangle)^2\rangle$ is the variance of the phase. If experimental data indicate that $\ln(E)$ vs q^2 is a straight line, which will generally be true for small values of q, then we know that the q^2 term is dominant in this region and we can calculate the variance $\sigma_x^2 = \langle(X - \langle X\rangle)^2\rangle$ from the slope of the straight line (*4*). In this linear region, we can write

$$E = e^{-2\pi^2 q^2 \sigma_X^2} \quad [14]$$

which is identical to Eq. [13]. Thus, we can calculate σ_X^2 from Eq. [14] either for Guassian phase distribution or for small values of q, where $\ln(E)$ vs q^2 is a straight line.

The phase variance in Eq. [13] depends on the velocity autocorrelation function $R_u(\tau)$ and the shape of the probing gradient waveform. This relationship can be explicitly written as

$$\sigma_\phi^2 = \gamma^2 \int_0^\infty \theta(t) \int_0^\infty R_u(t-s)\theta(s)dsdt \quad [15]$$

$$= 2\gamma^2 \int_0^T \theta(t) \int_0^t R_u(t-s)\theta(s)dsdt, \quad [16]$$

where we have defined $\theta(t) = \int_0^t g(s) = 0$, for $t \geq T$. Thus if the velocity autocorrelation function is known we can calculate σ_ϕ^2 and hence the signal attenuation. Equation [15] is in a convenient form to take the Fourier transform and have an expression for signal attenuation in terms of the velocity autocorrelation spectrum and the gradient waveform spectrum (*2*). If $R_u(\tau)$ can be written in terms of separable functions, then Eq. [16] can be further simplified. For example, if $R_u(t - s) = \sum_k A_k(t)A_k(s)$, then

$$\sigma_\phi^2 = 2\gamma^2 \sum_k \int_0^T \theta(t)A_k(t) \int_0^t \theta(s)A_k(s)dsdt. \quad [17]$$

A Mathematica program was used for such calculations. Any $R_u(\tau)$ that is a sum of functions of the form $\langle u^2\rangle e^{-|\tau|/\tau_a}\cos(\omega\tau)$ satisfies the separable requirement.

We consider a train of bipolar gradient pulse pairs whose polarity is chosen to probe spin dynamics. We have n such pairs in Fig. 1A. For such a pulse train, the apparent diffusion coefficient $D_a(\Delta)$ measured by NMR is defined by

$$E(q, \Delta, \delta) = e^{-4n\pi^2 q^2(\Delta - (\delta/3))D_a(\Delta)}. \quad [18]$$

$D_a(\Delta)$ can be calculated from Eq. [18] without any knowledge of $R_u(\tau)$. For any specific model of $R_u(\tau)$, we can theoretically relate $D_a(\Delta)$ to the parameters of $R_u(\tau)$. The factor n in the exponent (Eq. [18]) ensures that we have $D_a = D$ for any number n of bipolar pulses (*2*) for uncorrelated Brownian motion ($R_u(\tau) = 2D\delta(\tau)$).

The MRI experiment to measure diffusion consists of slice selection, followed by sensitizing the magnetization phase to motion, and imaging the slice. Magnetic field gradients for motion sensitivity should have zero total area and otherwise can have different patterns to probe motion properties (*2*). The common bipolar gradient (Fig. 1B), also known as a pulsed-field-gradient method, will be called a single-pulsed-gradient sequence (SPG). In Fig. 1C we have a SPG sequence repeated once, which we call a repeated single pulsed gradient sequence (RSPG). In Fig. 1D we have a flow compensated sequence, a sequence with its first moment zero ($\int tg(t)dt = 0$), which we call a compensated pulsed gradient sequence (CPG). If necessary, these sequences can be extended to n pulses to probe more complex velocity autocorrelation functions.

For the SPG sequence the intensity of any voxel is given by

$$E(q, \Delta, \delta) = Ke^{-4\pi^2 q^2(\Delta - \delta/3)D_S(\Delta)}, \quad [19]$$

where δ is the gradient pulse width, Δ the gradient pulse separation, and K a proportionality constant. $D_S(\Delta)$ is the apparent time-dependent diffusion coefficient. Its spatial distribution can be calculated by repeated imaging for different values of q, at fixed values of Δ and δ, followed by a voxel-by-voxel least-squares fit to Eq. [19].

For the RSPG sequence the apparent time-dependent diffusion coefficient $D_R(\Delta)$ is defined by

$$E(q, \Delta, \delta) = Ke^{-8\pi^2 q^2(\Delta - \delta/3)D_R(\Delta)}. \quad [20]$$

Similarly for the CPG sequence we define $D_C(\Delta)$ by

$$E(q, \Delta, \delta) = Ke^{-8\pi^2 q^2(\Delta - \delta/3)D_C(\Delta)}. \quad [21]$$

It follows from Eqs. [2], [14], and [17] that for the SPG sequence $D(\Delta) = (1 - (\delta/(3\Delta))D_S(\Delta)$. Thus by measuring $D_S(\Delta)$ by NMR we can calculate $D(\Delta)$. This relationship has made the PGSE technique very popular for probing diffusive motion.

Let us define $\theta_1(t) = \int_0^t g(s)ds$, for $0 \leq t \leq \Delta + \delta$, and zero otherwise. Then for the RSPG sequence $\theta(t) = \theta_1(t) + \theta_1(t - \Delta - \delta - \tau_m)$ and for the CPG sequence $\theta(t) = \theta_1(t) - \theta_1(t - \Delta - \delta - \tau_m)$ which, when substituted in Eq. [15], imply that

$$\sigma_\phi^2(RSPG) = 2[\sigma_\phi^2(SPG) + \gamma^2 \int_0^\infty \theta_1(t - \Delta - \delta - \tau_m) \times \int_0^\infty R_u(t - s)\theta_1(s)dsdt] \quad [22]$$

and

$$\sigma_\phi^2(CPG) = 2[\sigma_\phi^2(SPG) - \gamma^2 \int_0^\infty \theta_1(t - \Delta - \delta - \tau_m) \times \int_0^\infty R_u(t - s)\theta_1(s)dsdt]. \quad [23]$$

It follows from Eq. [13], the definition of the apparent diffusion coefficients (Eq. [18]), and Eqs. [22] and [23] that

$$D_S(\Delta) = \frac{D_R(\Delta) + D_C(\Delta)}{2} \quad [24]$$

for any velocity autocorrelation function. Another property of these apparent diffusion coefficients is that the two central gradient pulses overlap and cancel each other for the RSPG sequence (Fig. 1C) with infinitesimally small δ and τ_m, reducing the RSPG sequence to a SPG sequence. Thus for infinitesimally small δ and τ_m, $D_S(2\Delta) = D_R(\Delta)$.

The functional form of the three apparent diffusion coefficients can be calculated in terms of velocity autocorrelation parameters from Eqs. [13] and [15] and Eqs. [19]–[21]. If $R_u(\tau) = \langle u^2 \rangle e^{-|\tau|/\tau_c}$, then

$$D_S(\Delta) = D\left(1 + \frac{a}{\delta^2(\Delta - \delta/3)}\right), \quad [25]$$

$$D_R(\Delta) = D\left(1 + \frac{a + e^{-(\tau_m/\tau_c)}b/2}{\delta^2(\Delta - \delta/3)}\right), \quad [26]$$

$$D_C(\Delta) = D\left(1 + \frac{a - e^{-(\tau_m/\tau_c)}b/2}{\delta^2(\Delta - \delta/3)}\right), \quad [27]$$

where

$$a = -2\tau_c^2\delta + \tau_c^3(1 - e^{-(\delta/\tau_c)}) \times (2 - e^{-(\Delta/\tau_c)} + e^{-(\Delta-\delta)/(\tau_c)}), \quad [28]$$

$$b = \tau_c^3(1 - e^{-(\delta/\tau_c)})^2(1 - e^{-(\Delta/\tau_c)})^2, \quad [29]$$

and $D = \langle u^2 \rangle \tau_c$.

In Fig. 2 we compare the three apparent diffusion coefficients for a small δ and $\tau_m = 0$. All three apparent diffusion coefficients tend to the asymptotic diffusion coefficient D for $\tau_c \ll \Delta$. In other words, if the spin motion is uncorrelated in the time scale of our pulsed gradient sequence, then all three apparent diffusion coefficients measure the same quantity D. For highly correlated motion within the time Δ ($\tau_c \gg \Delta$) Eq. [27] implies that $D_C(\Delta)$ approaches zero for any Δ as τ_c tends to infinity. In other words, there is no attenuation in image intensity because of motion. This is the distinguishing feature of the compensated CPG sequence. It compensates for correlations in motion and increases sensitivity for correlation time measurements. In addition, for $\tau_c \gg \Delta$, we have $D_S(\Delta) = D_R(\Delta)/2 = \langle u^2 \rangle \Delta/2$, the ballistic ($\sigma_x^2 \propto \Delta^2$) short time motion of the O–U process.

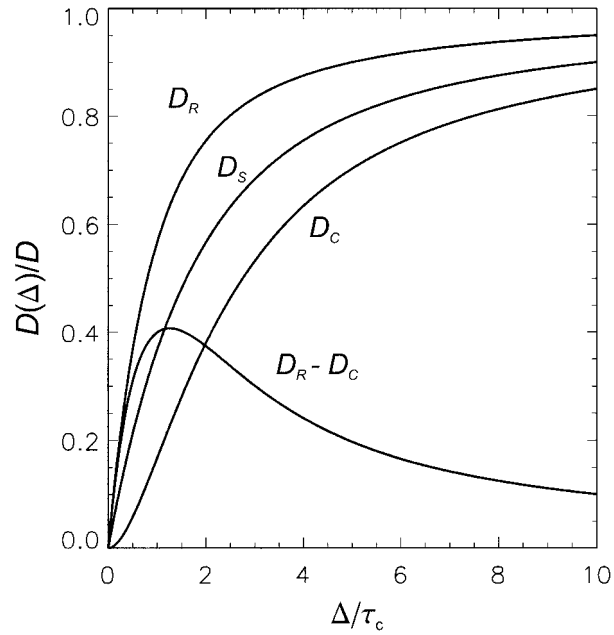

FIG. 2. Dependence on the ratio Δ/τ_c of the apparent time-dependent diffusion coefficient for the gradient sequences of Figs. 1B–1D for ideal gradients, $\delta = 0$, and the exponential velocity correlation function $R_u(\tau) = \langle u^2 \rangle e^{-(|\tau|/\tau_c)}$. For $\Delta \ll \tau_c$, the single (D_S) and repeated (D_R) pulsed gradients exhibit short time diffusive behavior which is linear, while the compensated sequence ($D_C \approx 0$) refocuses the magnetization for motions which appear deterministic over time Δ. This is evidenced by the difference ($D_R - D_C$), which collapses to D_R at short observation times. All three gradient sequences measure the same asymptotic diffusion $D = \langle u^2 \rangle \tau_c$ in the limit $\Delta \gg \tau_c$.

We have also plotted the normalized difference $(D_R(\Delta) - D_C(\Delta))/D$ of the apparent diffusion coefficients for the repeated and the compensated pulse sequences for $\delta = \tau_m = 0$ in Fig. 2. It is a measure of the spin phase refocusing by the CPG sequence and depends on the relative values of Δ and τ_c. The difference is a linear function of Δ for $\tau_c \gg \Delta$, because $D_C(\Delta) \to 0$ and $D_R(\Delta)$ is linear. It has the interesting property of having a maximum at $(\Delta/\tau_c) = 1.24$. It approaches zero for $\tau_c \ll \Delta$ because the particle motion appears random. Thus we immediately know the range of τ_c in our experiment from the difference of $D_R(\Delta)$ and $D_C(\Delta)$ as a function of Δ.

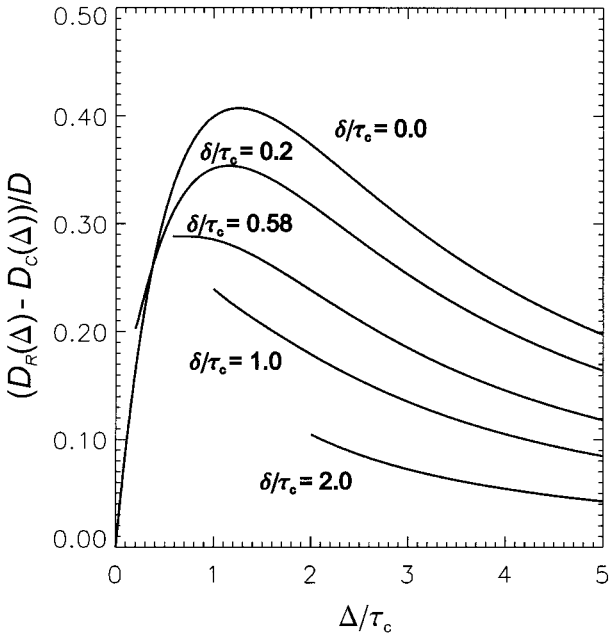

FIG. 3. Effect of the gradient pulse duration δ on the difference $D_R - D_C$ of the apparent diffusion coefficients measured for the repeated single and compensated pulsed gradient sequences as a function of the ratio Δ/τ_c. For $\delta/\tau_c \geq 0.58$ the difference is everywhere decreasing as a function of Δ/τ_c, providing an alternative means to determine the range of the correlation time.

Even though all curves were plotted for infinitesimally small δ in Fig. 2, the effect of finite δ can be considered by looking at the exact expression for the difference between $D_R(\Delta)$ and $D_C(\Delta)$,

$$A(\Delta, \tau_m) = D_R(\Delta) - D_C(\Delta) = \frac{De^{-(\tau_m/\tau_c)}b}{\delta^2(\Delta - \delta/3)}. \quad [30]$$

In Fig. 3 we plot $A(\Delta, \tau_m)/D$ for $\tau_m = 0$ with the experimental restriction of $\Delta \geq \delta$. The difference is a monotonically decreasing function of Δ for $(\delta/\tau_c) \geq 0.58$. Thus, if the experimental data show that $(D_R(\Delta) - D_C(\Delta))$ is decreasing everywhere with Δ for $\Delta \geq \delta$, then we know that $(\delta/\tau_c) \geq 0.58$. The sensitivity for measuring τ_c decreases with increasing δ/τ_c. It is best to be able to choose δ as small as possible and work near the maximum of $(D_R(\Delta) - D_C(\Delta))$. The available gradient strength limits the smallest that can be used because signal attenuation depends on $q = (\gamma g \delta)/(2\pi)$.

There is considerable flexibility in how to calculate D and τ_c from Eqs. [25]–[27] and the difference Eq. [30]. Here we discuss some of the possibilities and the analysis used in this work. Even if we had carried out only the SPG experiment (Eq. [25]) for a number of Δ values, we would in principle have sufficient data for calculating D and τ_c. In some experiments, such as our rotating cylinder experiment, D and τ_c are spatially varying. If the time Δ over which the motion is probed is large, then in this time the particles can move over regions of widely different D and τ_c, making it impossible to assume that their stochastic properties are stationary. At the top center of the flowing layer in our experiments the velocity was about 30 cm/s, so a particle moves 7.2 mm during the motion probing time of 24 ms ($2\Delta + 4\delta$), which is about 7 pixels at 1 mm spatial resolution. Therefore, we are measuring average particle dynamics over the region the particle moves in $2\Delta + 4\delta$. Smooth spatial variation of D and τ_c over these 7 pixels gives us added physical basis to trust the stationarity assumption.

We have seen from Eq. [24] that only two of these experiments are independent. We can extract the information of the third experiment from any two experiments. However, if the process is stationary over the total motion probing time, Eq. [24] is true. We note that with SPG the motion is probed for a time interval $\Delta + 2\delta$ (Fig. 1B), while for RSPG and CPG it is probed for time interval $2\Delta + 4\delta$. If all three experiments are done and Eq. [24] does not hold, then we know that particle motion statistics present over $\Delta + 2\delta$ are not the same over the $2\Delta + 4\delta$ interval, and we conclude that particle motion is not stationary during the experiment. Thus doing all three experiments and testing the validity of Eq. [24] gives us a check on the stationarity of the spin motion. Finally, the use of all three sequences increases the number of measurements for the same Δ from which to calculate D and τ_c and provide separation of the stochastic and deterministic motions relative to time scale Δ (*4*, *33*).

If τ_m is varied for fixed values of δ and Δ then Eq. [30] gives a simple method for calculating D and τ_c. However, if we do not vary Δ we forego the advantage of finding out whether the experiment was done near the sensitive part of Eq. [30], i.e., near the maximum in $A(\Delta, \tau_m)$. In this paper we have kept $\tau_m = 0$, δ constant, and varied Δ, starting from a minimum value of Δ which we call $\Delta_{\min}$ ($\geq\delta$). As mentioned earlier, this was done to probe whether we were at the sensitive region of Eq. [30]. We calculated τ_c from

$$\frac{A(\Delta)}{A(\Delta_{\min})} = \frac{(\Delta_{\min} - \delta/3)}{(\Delta - \delta/3)} \frac{(1 - e^{-(\Delta/\tau_c)})^2}{(1 - e^{-(\Delta_{\min}/\tau_c)})^2} \quad [31]$$

by nonlinear least squares fit. This ratio is independent of D. Once τ_c is known, D can be calculated from Eqs. [25]–[27] by a linear fit.

So far, we have discussed the method for calculating D and τ_c in detail for $R_u(\tau) = \langle u^2 \rangle e^{-|\tau|/\tau_c}$. To demonstrate the ability of our method to handle more complex velocity autocorrelation functions we present the example of a velocity autocorrelation modeled as a sum of exponentials. Such a velocity autocorrelation function is relevant to a particle in a high density fluid undergoing "caged diffusion" and particles diffusing in a box. $R_u(\tau)$ can become negative because the particle suffers reflection on collision with the walls (*38*). Different analytical models for these types of velocity autocorrelation functions have been discussed in the context of molecular dynamics by Boon

and Yip (*38*). Negative velocity autocorrelation functions have also been seen in porous media flow studies (*39*) and in computer simulations of granular fluids in the rapid flow, gas regime (*40*). One simple model is that of a sum of two exponentials with one of the coefficients being negative (*41*). Again the apparent diffusion coefficients D_S, D_R, and D_C can be easily calculated in terms of the parameters describing $R_u(\tau)$. Thus if

$$R_u(\tau) = \sum_k c_k e^{-(|\tau|/\tau_k)}, \qquad [32]$$

then

$$\langle u^2 \rangle = \sum_k c_k, \qquad \tau_c = \frac{\sum_k c_k \tau_k}{\sum_k c_k},$$

and $D = \sum_k c_k \tau_k$. The coefficients c_k do not have to be all positive, although their sum $\langle u^2 \rangle$ must be. In this case the equations corresponding to Eqs. [25]–[27] are

$$D_S = D + \frac{\sum_k c_k \tau_k a_k}{\delta^2(\Delta - \delta/3)}, \qquad [33]$$

$$D_R = D + \frac{\sum_k c_k \tau_k (a_k + e^{-(\tau_m/\tau_k)} b_k/2)}{\delta^2(\Delta - \delta/3)}, \qquad [34]$$

and

$$D_C = D + \frac{\sum_k c_k \tau_k (a_k - e^{-(\tau_m/\tau_k)} b_k/2)}{\delta^2(\Delta - \delta/3)}. \qquad [35]$$

a_k and b_k in Eqs. [33]–[35] can be appropriately obtained from the definitions in Eqs. [28] and [29]. For this more complex $R_u(\tau)$, we must estimate $2n$ parameters for a sum of n exponentials from NMR data, a much harder problem.

Let us consider a simple model for $R_u(\tau)$ in the case of particles diffusing with an O–U process within parallel plates of separation d (*41*),

$$R_u(\tau) = D_u \left(\frac{1}{\tau_u} e^{-(|\tau|/\tau_u)} - \frac{1}{\tau_w} e^{-(|\tau|/\tau_w)} \right). \qquad [36]$$

In this equation τ_u is the correlation time for the unrestricted process and D_u the unrestricted asymptotic diffusion coefficient. Qualitatively τ_u is a measure of particle dynamics and the collision with the walls is modeled by τ_w. The negative sign before the second exponential models the reflection at the walls. τ_w is of the order of d^2/D_u, the average time a particle needs to diffuse across the separation between the walls. An interesting property of Eq. [36] is that the asymptotic D as defined by Eq. [4] and the average correlation time τ_c are both zero. This is because the particle movements are bounded by wall restrictions, which makes $\langle (x(\Delta) - x(0))^2 \rangle$ also bounded, and as the time Δ goes to infinity D tends to zero (Eq. [2]). In Fig. 4 we plot the apparent diffusion coefficients D_S, D_R, and D_C as a function of Δ/τ_u for $\tau_w/\tau_u = 16$. In a system described by Eq. [36] there is always a crossover point at $\Delta = \Delta_c$ as shown in Fig. 4A, such that for $\Delta \geq \Delta_c$, $D_C \geq D_R$. This occurs because the spin magnetization phase gets refocused due to reflections at the wall or particle cage and not because of the bipolar gradient polarity being reversed as in the CPG sequence. In Fig. 4B we show the expected behavior that at long observation times the three apparent diffusion coefficients go to zero asymptotically. This example again demonstrates the advantage of carrying out experiments with the RSPG and the CPG sequences. If we were to see that $D_R(\Delta)$ has become smaller than $D_C(\Delta)$ for some Δ, then we know that the particle velocities have reversed in the time between the first and the second bipolar gradient pulses. This could happen because of wall reflections, as in the above example of restricted diffusion in a box or particle cage, or due to vortices in a flow.

EXPERIMENT

The experimental system consisted of a horizontal 70-mm i.d. cylinder half-filled with 2-mm oil-filled, hard plastic spherical beads and rotated at 2.3 rad/s (22 rpm) at an ambient temperature of 25°C (Fig. 5). The MRI experiment was done in a 31-cm, 1.9 T Oxford magnet with a TECMAG imager/spectrometer. We took a 20-mm thick transverse slice and made an image of the cylinder cross-section with 1-mm by 1-mm in-plane resolution. In this paper we will discuss only the axial component of the velocity autocorrelation function. This is the most straightforward component to consider because of the absence of any average velocity in the axial direction. Clearly, this method will also apply to measurements of correlation times of velocity components in other directions.

The pulse sequence used in these experiments is shown in Fig. 6. Six π pulses were used to refocus the effect of motion in the presence of magnetic field inhomogeneities. The even number of π pulses ensures that the first moment of the background gradient is zero and the phase acquired by spins moving with constant velocity in the presence of these gradients is also zero (*21*). This refocussing of background gradients minimizes signal loss and enhances the signal-to-noise ratio for calculating the apparent diffusion coefficients. There is some unavoidable signal loss from spins in voxels that experience acceleration, on average. This loss was minimized by keeping the time between the π pulses short, and increasing the time for the gradient pulse separation by going from an initial 2π pulse sequence to the 6π pulse sequence used.

The diffusion coefficient and the correlation time for the axial (Z) component of velocity fluctuations were measured by

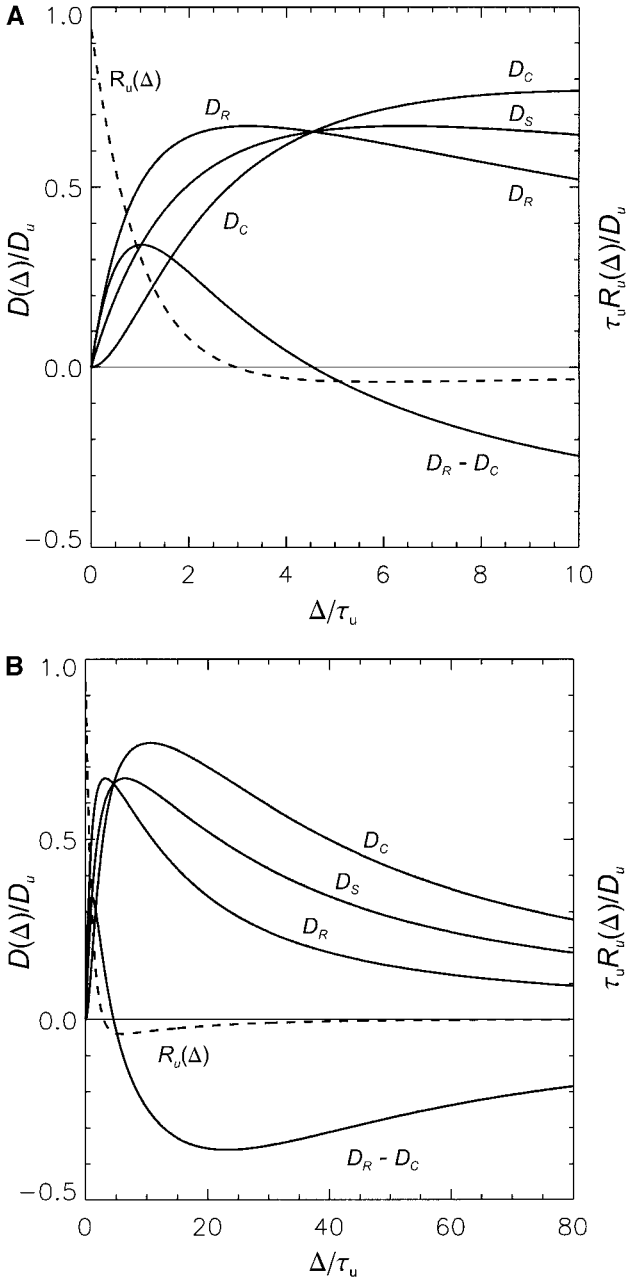

FIG. 4. Dependence on the ratio Δ/τ_u of the apparent time-dependent diffusion coefficient for the gradient sequences of Figs. 1B–1D for ideal gradients, $\delta = 0$, and the velocity correlation function $R_u(\tau) = D_u[(1/(\tau_u)e^{-|\tau|/\tau_u} - (1/\tau_w)e^{-|\tau|/\tau_w}]$ with $\tau_w/\tau_u = 16$. $R_u(\tau)$ exhibits negative correlation for $\Delta/\tau_u > 3$ because particle velocity is reversed on collision with the walls. In (A), at larger values of Δ/τ_u, D_C becomes larger than D_R because of wall reflections; (B) shows the behavior of the apparent diffusion coefficients at longer times. All three apparent diffusion coefficients approach zero as $\Delta \to \infty$ because the position variance is bounded.

choosing the motion sensitizing gradients in Fig. 6 to be in the axial direction. The diffusion coefficient and correlation time in the transverse plane can be measured by choosing diffusion sensitizing gradients in the (X, Y) directions and the full

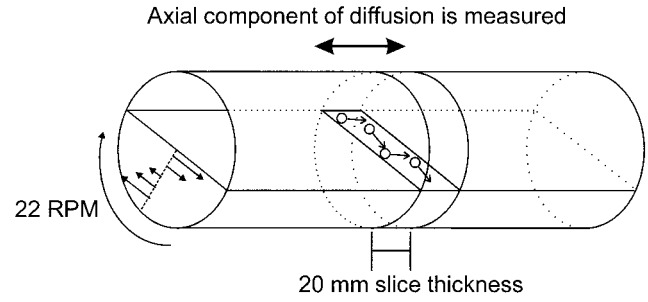

FIG. 5. Schematic of the granular flow experimental geometry. In this experiment we present data for the diffusive motion in the axial direction of a half-filled rotating cylinder as a function of the length l parallel to the free surface and depth h perpendicular to the free surface. The particles undergo shear flow in a lens shaped layer near the free surface and are returned to the top of the flow by solid body rotation, as depicted by the arrows for velocity in the left end of the cylinder.

diffusion tensor by suitable combinations of the gradients. The in-plane particle velocity images in the horizontal and the vertical direction and the axial velocity were also measured by the phase method (*21*) with three velocity encoding steps. The velocity sensitivity was 0.24 m/s per π radians of phase shift. The mean velocity in the axial direction was found to be zero. The spatial dependence of the three apparent diffusion coefficients $D_S(\Delta)$, $D_R(\Delta)$, $D_C(\Delta)$ were measured for a fixed $\delta =$ 2.048 ms and Δ of 2.75, 6.31, and 8.06 ms. Each apparent

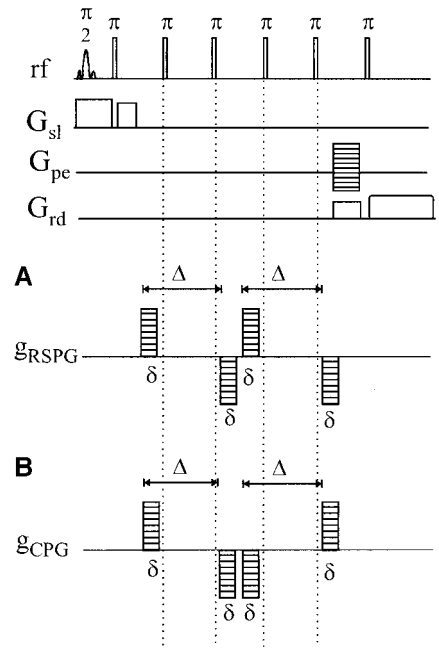

FIG. 6. The imaging pulse sequence used to measure the axial diffusion in the rotating cylinder. Six π pulses minimize the echo time and provide even echo refocusing of magnetization phase due to particle motion in background gradients. Motion sensitizing gradient pulse trains are presented for (A) the repeated single pulsed gradient (RSPG) and (B) the compensated pulsed gradient (CPG) experiments.

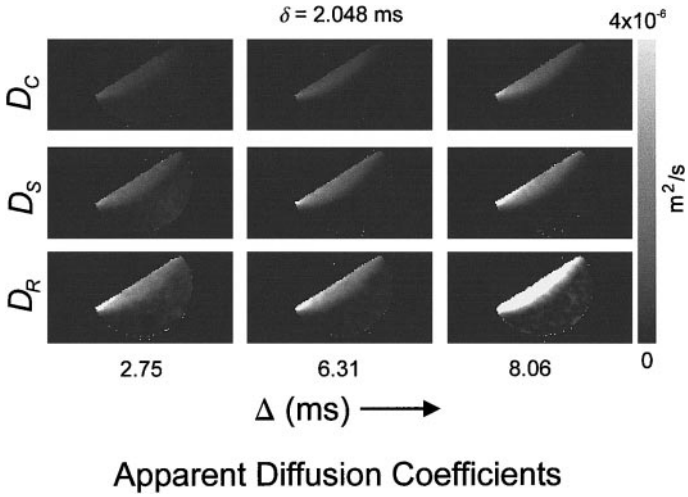

FIG. 7. Grayscale NMR images of the apparent diffusion coefficient measured in the granular flow for the CPG (D_C), SPG (D_S), and RSPG (D_R) sequences for displacement observation times $\Delta = 2.75$, 6.31, and 8.06 ms and a fixed pulsed gradient duration $\delta = 2.048$ ms. The image intensity is proportional to the amplitude of the apparent diffusion coefficient and all images are scaled the same with maximum intensity (white) being 4×10^{-6} m^2/s.

diffusion coefficient image was measured by stepping the gradients in 5 equal steps and fitting the data voxel-by-voxel to Eqs. [25]–[27]. The five steps provided a check on the linearity of $\ln(E)$ vs q^2 plot. The range was optimized by doing initial experiments with 16 steps to our maximum gradient strength and selecting a suitable subset of 5 steps for these experiments. This gives us 9 apparent diffusion coefficient images from which to calculate D and τ_c by nonlinear least squares fitting.

RESULTS

The nine apparent axial diffusion coefficient images, referred to in the prevoius paragraph, are shown in Fig. 7. The three columns represent increasing observation times Δ from left to right (2.75, 6.31, and 8.06 ms). The rows represent the three different gradient pulse sequences shown in Fig. 1, in order of greater signal attenuation or apparent diffusion (D_C, D_S, and D_R, corresponding to CPG, SPG, and RSPG). In all images, the gradient pulse length δ was 2.048 ms. In order to make apparent the variation in the data for the different gradient sequences we scaled the intensity identically for all images so that the contrast is appropriate for the upper left image, but in so doing, we have saturated the more intense images toward the lower right. Nevertheless, the spatial variation of the apparent diffusion coefficient is clearly evident in the intermediate images.

A consistent feature of all the data is the increase in axial diffusion with distance along the flow direction, from right to left in these images, as has already been reported (*7*, *8*). The apparent diffusion increases with Δ for all three sequences while it increases for each Δ in going from CPG to SPG to RSPG, indicating that τ_c is of the same order as Δ. As a result, we are able to calculate τ_c from Eqs. [25]–[29].

Figure 8 shows quantitative plots of the apparent axial diffusion coefficients along two selected lines from the center column ($\Delta = 6.31$ ms) of Fig. 7. The two selected lines are the perpendicular bisector of the free surface and a line parallel to the free surface but 1 mm below it, as shown in a schematic diagram to the right. We also plot the average of D_R and D_C as a dotted line and it is identical, within experimental errors, to D_S. This agreement confirms that particle dynamics have not violated the stationary assumption during the motion-probing time ($2\Delta + 4\delta$).

There are minor differences in the relative amplitudes of D_C and D_R between Fig. 4 of Ref. (*8*) and our Fig. 8A in deeper regions of the flowing layer. The rotation rates were the same in the two experiments but the profiles for the two figures are at slightly different places in the flow. These differences are not significant and further experiments will be done to clarify the nature of particle dynamics in this region. However, the fact that independent measurements of D_C, D_S, and D_R satisfy Eq. [24] provides a consistency check that gives us confidence in the present results.

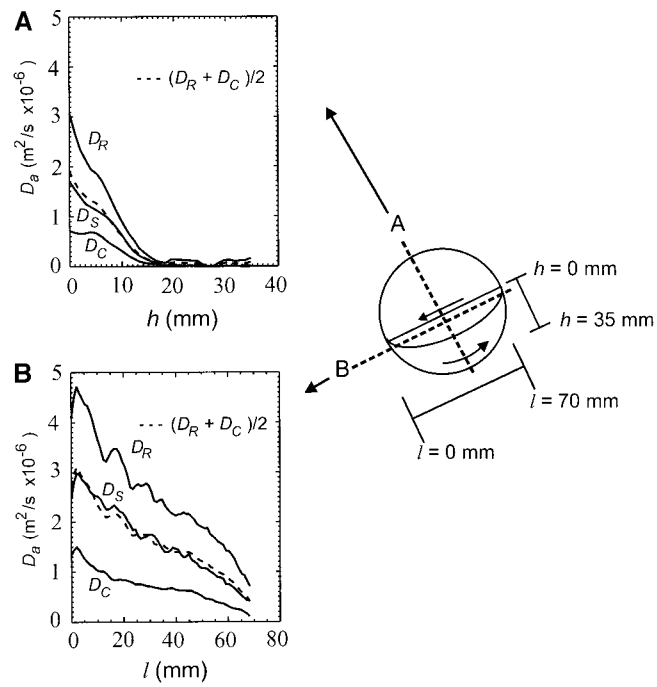

FIG. 8. Quantitative plots of the spatial dependence of the apparent diffusion coefficients measured by CPG (D_C), SPG (D_S), RSPG (D_R), and the average $(D_R + D_C)/2$ as a function of (A) the depth in the flowing layer h at the center of the flow $l = 35$ mm and (B) the distance l along the flow at a depth of $h = 1$ mm. The data are from the images of Fig. 7 for $\Delta = 6.31$ ms. The variation of diffusion with depth is elucidated by the curves and is different for the CPG sequence which is almost constant below the free surface, than for the RSPG and SPG sequences which have their maxima very near the free surface.

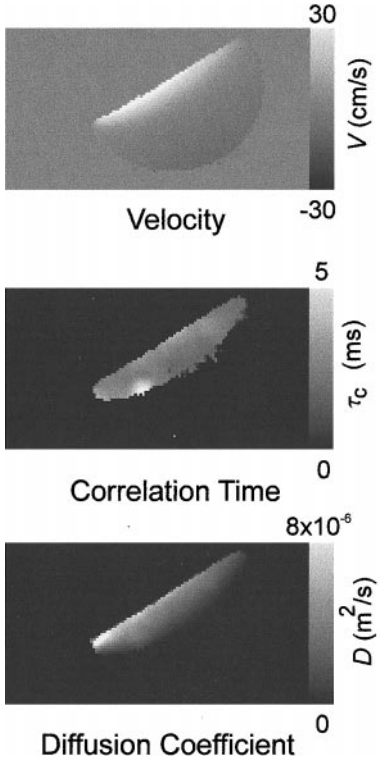

FIG. 9. Images of the in-plane velocity V, the axial correlation time τ_c, and the axial diffusion coefficient. The axial correlation time and diffusion coefficient images are calculated from the NMR data of Fig. 7.

The resulting axial correlation time image, calculated from the nine images of Fig. 7, is shown in Fig. 9, together with the image of the axial diffusion coefficient $D = \langle u^2 \rangle \tau_c$ and the image of the average velocity component parallel to the free surface, obtained by the phase method (*2, 21*) with the motion sensitizing gradients in the x–y plane. The velocity image is approximately symmetric about the center of the cylinder, i.e., particles speed up to the center and slow down past it, at any given depth in the flowing layer. At the same time, the flow velocity decreases with increasing depth, until it reaches zero at the boundary with the solid body region. The diffusion image, like the apparent diffusion images of Fig. 7, shows that D increases monotonically as a function of distance traveled down the flowing layer. The correlation time image does not scale directly with either the D or the velocity over the entire fluidized region and further experiments are being done at different rotation rates to asses these differences.

The axial correlation time τ_c, together with the axial diffusion coefficient D, and the in-plane velocity V, along the two specific directions described in Fig. 8, are shown in Figs. 10 and 11. Figure 10 shows these functions along the perpendicular bisector of the free surface (at $l = 35$ mm), whereas Fig. 11 shows them along a line parallel to the free surface and 1 mm below it (at $h = 1$ mm), corresponding to the apparent diffusion projections of Fig. 8A.

Figure 10 shows that the velocity profile is linear in the solid body region, as expected. It departs from the linear dependence quadratically as the particles start to move relative to each other away from the solid body region but the quadratic dependence is reduced as the free surface is approached, approximating a linear dependence (*7*). The diffusion coefficient D, negligibly small in the solid body region, increases approximately quadratically, as well, but seems to maintain this dependence all the way to the free surface. The axial correlation time τ_c is indeterminate in the solid body region but seems to assume a nonzero value of approximately 1.8 ms as soon as there is a measurable flow of particles at around $h = 14$ mm. It increases approximately quadratically from there to the free surface where it is about 3.5 ms, reflecting more energetic collisions that result in longer free flight times.

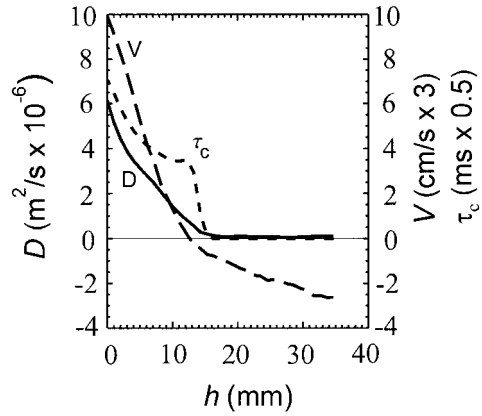

FIG. 10. Profiles from the data of Fig. 9 for the axial diffusion coefficient D, the correlation time τ_c, and longitudinal velocity V as a function of the depth below the free surface, h, at the center of the free surface, $l = 35$ mm. The axial correlation time τ_c is indeterminate in the solid body region due to the small values of the apparent diffusion coefficient measured.

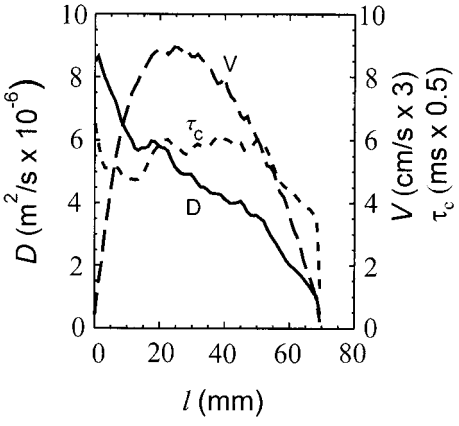

FIG. 11. Profiles from the data of Fig. 9 for the axial diffusion coefficient D, the correlation time τ_c, and the longitudinal velocity V as a function of the position along the free surface, l, at a depth of $h = 1$ mm. The axial correlation time τ_c does not scale with either V or D. In fact, it is virtually constant for most of the flow, after the initial rise from about 1.8 to 3 ms over the first 20 mm of the flowing layer.

Figure 11 shows that the same three parameters are much more diverse along a line 1 mm below the free surface, corresponding to the apparent diffusion coefficient projections of Fig. 8B. The in-plane velocity V is a skewed parabola with its peak shifted to the lower half of the flow while the diffusion coefficient D increases monotonically from the top to the bottom of the flow. In contrast, the correlation time τ_c starts from a nonzero value ($\sim$1.8 ms) at the top of the flowing region, increases approximately linearly for the first 20 mm, and remains steady at a value about 3 ms for the rest of the way. Thus, neither D nor τ_c scale with V over the length of the free surface.

At the top-center of the flowing layer (l = 35 mm and h = 1 mm), where the two lines chosen for analysis intersect (Fig. 8), the longitudinal velocity V is 0.29 m/s, the diffusion coefficient D is 5.5×10^{-6} m^2/s, and the correlation time is around 3 ms. This results in a velocity fluctuation intensity or granular temperature $\langle u^2 \rangle$ of 1.8×10^{-3} m^2/s^2.

CONCLUSIONS

A general parametric method, using NMR, has been developed for measuring velocity autocorrelation functions. The method can be applied to such functions which can be expressed as a sum of exponentials. The method was applied to the problem of characterizing the correlation time in a heterogeneous granular flow in a half-filled horizontal rotating cylinder, an Ornstein–Uehlenbeck process with

$$R_u(\tau) = \langle u^2 \rangle e^{-(|\tau|/\tau_c)}.$$

Heretofore, no experimental technique had yielded such data in bulk granular flows; the closest anyone having come to such a measurement was the diffusing wave spectroscopy method of Durian's group (*17*), which has excellent temporal resolution but poor spatial resolution and depth of field that is limited by the number of light reflections by the particles. Their method also does not select a velocity component to study but measures the average of fluctuations in all directions.

We have shown that the correlation time τ_c of the velocity in the axial direction, perpendicular to the plane containing the flow, is in the range of milliseconds and does not scale with either the particulate diffusion coefficient nor the in-plane average velocity over the entire fluidized region. The diffusion coefficient D is some three orders of magnitude greater than the molecular diffusion coefficient for water, due to the relatively long free-flight times of the particles which is reflected in the long τ_c values. We can get a spatial map of granular temperature from the spatial distribution of τ_c and D; its typical range for this particular system goes up to a few times 10^{-3} m^2/s^2.

Thus, we have presented a new NMR method to study correlations of random processes. This approach should have applications not only in granular flow but also in turbulence, porous media flow, and various suspension flows. As a byproduct, we have shown that the venerable Stejskal–Tanner sequence can be applied to macroscopic diffusion in granular flows, in addition to molecular diffusion as it has been applied for more than three decades.

ACKNOWLEDGMENTS

This research was supported by the Engineering Research Program of the Office of Basic Energy Sciences, Department of Energy, under Grant DE-FG03-98ER14912. We thank Eiichi Fukushima, Steve Altobelli, and Dean Kuethe for many discussions and Cathy Clewett for assistance in drawing the figures.

REFERENCES

1. E. O. Stejskal and J. E. Tanner, Spin diffusion measurements: Spin echoes in the presence of a time-dependent field gradient, *J. Chem. Phys.* **42,** 288–292 (1965).
2. P. T. Callaghan, "Principles of Nuclear Magnetic Resonance Microscopy," Chaps. 6–8, Oxford Univ. Press, New York, (1991).
3. P. T. Callaghan and J. Stepisnik, Generalized analysis of motion using magnetic field gradients, *Adv. Opt. Magn. Reson.* **19,** 325–388 (1996).
4. P. T. Callaghan, S. L. Codd, and J. D. Seymour, Spatial coherence phenomena arising from translational motion in gradient spin echo experiments, *Concepts in Magn. Reson.* **11,** 181–202 (1999).
5. M. Nakagawa, S. A. Altobelli, A. Caprihan, and E. Fukushima, Non-invasive measurements of granular flows by magnetic resonance imaging, *Exp. Fluids* **16,** 54–60 (1993).
6. K. M. Hill, A. Caprihan, and J. Kakalios, Axial segregation of granular media rotated in a drum mixer: Pattern evolution, *Phys. Rev. E* **56,** 4386–4393 (1997).
7. K. Yamane, M. Nakagawa, S. A. Altobelli, T. Tanaka, and Y. Tsuji, Steady particulate flows in a horizontal rotating cylinder, *Phys. Fluids* **10,** 1419–1427 (1998).
8. J. D. Seymour, A. Caprihan, S. A. Altobelli, and E. Fukushima, Pulsed gradient spin echo nuclear magnetic resonance imaging of diffusion in granular flow, *Phys. Rev. Lett.* **84,** 266–269 (2000).
9. H. M. Jaeger, S. R. Nagel, and R. P. Behringer, Granular solids, liquids, and gases, *Rev. Mod. Phys.* **68,** 1259–1273 (1996).
10. S. B. Savage and D. J. Jeffrey, The stress tensor in a granular flow at high shear rates, *J. Fluid Mech.* **110,** 255–272 (1981).
11. J. T. Jenkins and M. W. Richman, Boundary conditions for plane flows of smooth, nearly elastic, circular disks, *J. Fluid Mech.* **171,** 53–69 (1986).
12. P. K. Haff, Grain flow as a fluid mechanical phenomenon, *J. Fluid Mech.* **134,** 401–430 (1983).
13. S. B. Savage and R. Dai, Studies of granular shear flows wall slip velocities, 'layering' and 'self-diffusion,' *Mech. Mater.* **16,** 225–238 (1993).
14. S. B. Savage, Disorder, diffusion and structure formation in granular flows, *in* "Disorder and Granular Media" (D. Bideau and A. Hansen, Eds.), pp. 255–284, Elsevier, Amsterdam (1993).
15. O. Zik, D. Levine, S. G. Lipson, S. Shtrikman, and J. Stavans, Rotationally induced segregation of granular materials, *Phys. Rev. Lett.* **73,** 644–647 (1994).

16. K. M. Hill and J. Kakalios, Reversible axial segregation of binary mixtures of granular materials, *Phys. Rev. E* **49,** 3610–3613 (1994).
17. N. Menon and D. J. Durian, Particle motions in a gas-fluidized bed, *Phys. Rev. Lett.* **79,** 3407–3410 (1997).
18. R. Kubo, M. Toda, and N. Hashitsume, "Statistical Physics II, Non Equilibrium Statistical Mechanics," Springer Series, Solid-State Sci., Vol. 30, Springer Verlag, Berlin/New York (1991).
19. J. P. Bouchaud and A. Georges, Anomalous diffusion in disordered media: Statistical mechanisms, models and physical applications, *Phys. Rep.* **195,** 127–293 (1990).
20. J. Stepisnik, NMR measurement and Brownian movement in the short-time limit, *Physica B* **198,** 299–306 (1994).
21. E. Fukushima, Nuclear magnetic resonance as a tool to study flow, *Annu. Rev. Fluid Mech.* **31,** 95–123 (1999).
22. H. Y. Carr and E. M. Purcell, Effects of diffusion on free precession in nuclear magnetic resonance experiments, *Phys. Rev.* **94,** 630–638 (1954).
23. P. G. deGennes, Theory of spin echoes in a turbulent fluid, *Phys. Lett. A* **29,** 20–21 (1969).
24. P. T. Callaghan and J. Stepisnik, Frequency-domain analysis of spin motion using modulated-gradient NMR, *J. Magn. Reson. A* **117,** 118–122 (1995).
25. J. H. Gao and J. C. Gore, Turbulent flow effects on NMR imaging: Measurement of turbulent intensity, *Med. Phys.* **18,** 1045–1051 (1991).
26. D. O. Kuethe and J. H. Gao, NMR signal loss from turbulence: Models of time dependence compared with data, *Phys. Rev. E* **51,** 3252–3262 (1995).
27. D. L. Koch and J. F. Brady, A non-local description of advection-diffusion with application to dispersion in porous media, *J. Fluid Mech.* **180,** 387–403 (1987).
28. J. D. Seymour and P. T. Callaghan, "Flow Diffraction" structural characterization and measurement of hydrodynamic dispersion in porous media by PGSE NMR, *J. Magn. Reson. A* **122,** 90–93 (1996).
29. J. J. Tessier, K. J. Packer, J.-F. Thovert, and P. M. Adler, NMR measurements and numerical simulation of fluid transport in porous solids, *AIChE J.* **43,** 1653–1661 (1997).
30. J. D. Seymour and P. T. Callaghan, Generalized approach to NMR analysis of flow and dispersion in porous media, *AIChE J.* **43,** 2096–2111 (1997).
31. M. H. G. Amin, S. J. Gibbs, R. J. Chorley, K. S. Richards, T. A. Carpenter, and L. D. Hall, Study of flow and hydrodynamic dispersion in a porous solid by pulsed-field-gradient magnetic resonance, *Proc. R. Soc. London, Ser. A* **453,** 489–513 (1997).
32. B. Manz, P. Alexander, and L. F. Gladden, Correlations between dispersion and structure in porous media probed by nuclear magnetic resonance, *Phys. Fluids* **11,** 259–267 (1999).
33. S. L. Codd, B. Manz, J. D. Seymour, and P. T. Callaghan, Taylor dispersion and molecular displacements in Poiseuille flow, *Phys. Rev. E* **60,** R3491–R3494 (1999).
34. A. Ding and D. Candela, Probing non-local tracer dispersion in flows through random porous media, *Phys. Rev. E* **54,** 656–660 (1996).
35. P. P. Mitra and B. I. Halperin, Effects of finite gradient-pulse widths in pulsed-field-gradient diffusion measurements, *J. Magn. Reson. A* **113,** 94–101 (1995).
36. S. Stapf, R. A. Damion, and K. J. Packer, Time correlations in fluid transport obtained by sequential rephasing gradient pulses, *J. Magn. Reson.* **137,** 316–323 (1999).
37. P. T. Callaghan and B. Manz, Velocity exchange spectroscopy, *J. Magn. Reson. A* **106,** 260–265 (1994).
38. J. P. Boon and S. Yip, "Molecular Hydrodynamics," Chap. 3, Dover, New York (1980).
39. N. C. Irwin, R. A. Greenkorn, S. A. Altobelli, and J. H. Cushman, Examination of transport theory of arbitrary order in velocity variance by MRI, *AIChE J.* **45,** 1351–1354 (1999).
40. T. P. C. van Noije and M. H. Ernst, Mesoscopic theory of granular fluids, *Phys. Rev. Lett.* **79,** 411–414 (1997).
41. J. Stepisnik, Spin echo attenuation of restricted diffusion as a discord of spin phase structure, *J. Magn. Reson.* **131,** 339–346 (1998).